

Review

Detailed structural and electrical characterization of plated crystalline silicon solar cells

C. Dang^{a,b,*}, R. Labie^a, E. Simoen^{a,c}, J. Poortmans^{a,b,d}^a Imec, Kapeldreef 75, 3001 Leuven, Belgium^b KU Leuven, Department Elektrotechniek – ESAT, Kasteelpark Arenberg 10, 3001 Leuven, Belgium^c Gent University, Krijgslaan 281 S1, 9000 Gent, Belgium^d UHasselt, Campus Diepenbeek, Agoralaan-gebouw D, 3590 Diepenbeek, Belgium

ARTICLE INFO

Keywords:

PERC cells

Laser ablation

Ni/Cu/Ag plating

Defects

Reliability

Diffusion

ABSTRACT

In this paper a detailed study on the electrical characteristics of Ni/Cu/Ag plated p-type Passivated Emitter Rear Contact (PERC) silicon solar cells is reported. By comparing the cell performance of different cell groups, pseudo Fill Factor (pFF) degradation by laser-induced defects, is observed. High-power (hard) laser ablated cells exhibit a lower efficiency and faster degradation with thermal ageing. We also present structural and electrical characterization to further visualize and identify the responsible defects, which turn out to be laser-ablation-induced dislocations, penetrating the silicon emitter and base. Increasing the laser fluence gives rise to a higher dislocation density. These dislocations are further confirmed as active generation-recombination centers by Deep Level Transient Spectroscopy (DLTS) analysis. The laser ablation induced dislocations are unavoidable because even at insufficient laser fluence (0.48 J/cm^2) to fully open the dielectric stack, the density is already at the level of $10^6/\text{cm}^2$. A substitutional nickel peak is also detected by DLTS, suggesting nickel diffusing into the silicon base during the sinter step. Whereas no copper levels are found in the p-type silicon base by DLTS even after thermal aging at 235°C .

1. Introduction

In recent years, developing an improved method for the metallization of silicon solar cells has been extensively studied. In the commercial solar cell market, the contact formation using Ag screen printing is the dominant technology as it is simple and suitable for mass production. However, this metallization has the disadvantage in having a low aspect ratio and high contact resistance therefore limiting the solar cell efficiency. The current trends with Ag screens involve using narrow opening width, smaller wire diameter and high opening fractions [1,2]. However, this reduces the screen lifetime and yields higher finger resistance as the printed amount is reduced. On the other hand, the advanced fine line printing techniques often require expensive screens and two-step printing, which lead to higher yield losses due to alignment needs and wafer breakage. All these factors of screen printing limit reductions in solar cell manufacturing costs. Besides that, Ag is an expensive and noble material and hence is subjected to a high price volatility. The mounting cost of silver pastes and decreasing silicon wafer thickness encourages silicon solar cell manufacturers to develop alternative metallization techniques that reduce the usage of Ag and get rid of the pressing process of screen printing while still having a

compatible solar cell performance.

The plated Cu/Ni has been considered as one of the most viable candidates for future contact technology for silicon solar cells. A plated Cu/Ni contact is known to have a high conductivity and low contact resistance. Copper's conductivity is compatible with silver while its raw material cost is nearly a hundred times smaller [3]. This is an important factor for cost reduction compared to the current technology. On the other hand, Cu has been widely used in Si Ultra Large Scale Integration (ULSI) due to its low resistivity and good resistance to electromigration [4].

Therefore, the plated Cu/Ni contact scheme not only presents solution to the issues associated with Ag screen printed contacts but also shows absolute efficiency gain of 0.5% [5].

However, it is also well known that Cu is a fast diffuser into Si and can act as a deep level impurity [6]. The diffused Cu can form traps which reduce the carrier lifetime and increase the leakage current once they are present near a p-n junction. To prevent the Cu diffusion, a diffusion barrier, such as a plated Ni layer is often used between Cu and silicon [7–10]. The Ni silicide which forms by annealing has a low contact resistance and acts as adhesion layer. Using Ni/Cu plating techniques is a good solution to improve the cell efficiency also because

* Corresponding author at: KU Leuven, Department Elektrotechniek – ESAT, Kasteelpark Arenberg 10, 3001 Leuven, Belgium.
E-mail address: dangchi@imec.be (C. Dang).

of less shading loss. By using laser ablation to open the passivation layer before plating, it is possible to achieve a width of less than 15 μm . However, despite these advantages, a final acceptance by the c-Si Photovoltaic (PV) community for introducing Cu in solar cell processing can only take place after thorough reliability results and an estimation for the module's lifetime.

In this study, thermal ageing testing for the p-type PERC cells with shallow emitter and front Ni/Cu metallization is discussed. This is complemented by a characterization of the electrically active defects, based on Scanning Electron Microscopy (SEM) and effective lifetime measurements Bias Temperature Instability (BTI). The second part of the paper takes a closer look at the electrical characteristics of the cells before and after thermal ageing, using Deep Level Transient Spectroscopy (DLTS).

2. Experimental details

2.1. p-PERC device fabrication

In this work, large area ($156 \times 156 \text{ mm}^2$) p-type, $1-3 \Omega \text{ cm}$, magnetic Czochralski (CZ) Si wafers, with starting thickness of 180 μm , were used. After random pyramid texturing for the front by KOH texture and inline rear polishing by HF/HNO₃, the wafers were processed according to the process sequence given in Fig. 2.

Prior to POCl₃ diffusion, the silicon wafers were subjected to a full Radio Corporation of America (RCA) clean in order to remove organic and metallic contamination before the fabrication process. A 2% HF solution was applied to remove phosphorus silicate glass, which formed during the POCl₃ diffusion step. After the Sulfuric Acid and hydrogen Peroxide Mixture (SPM)/HF clean, dry thermal oxidation was employed in order to drive-in phosphorus atoms in the Si bulk, forming thus a 0.5 μm deep homogeneous n⁺ emitter with a sheet resistance of $120 \Omega/\text{sq}$ and low surface concentration ($N_s < 10^{20} \text{ cm}^{-3}$). Subsequently, the POCl₃ diffusion emitter was passivated with a Plasma-Enhanced Chemical Vapor Deposition (PECVD) SiN_x:H layer, and at the rear a PECVD SiN_x:H was applied on top of the CVD SiO₂ diffusion mask.

For the rear dielectric stack, contact opening was formed on all cells by Ultra-Violet (UV) (355 nm) nanosecond laser ablation with a fixed pitch of 500 μm and an opened diameter of approximately 30 μm . Subsequently, 2 μm of aluminum was deposited by physical vapor

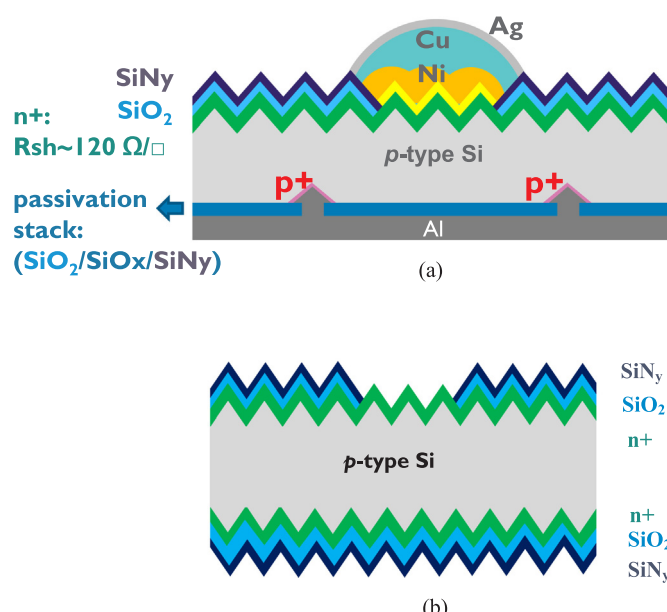


Fig. 1. (a) p-type PERC cell structure, (b) defect visualization and lifetime test structure.

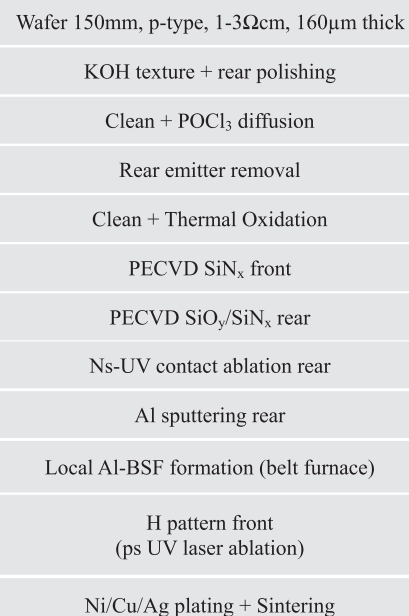


Fig. 2. Process sequence for i-PERC cells.

deposition (PVD) onto the rear surface, followed by a firing step in an inline belt furnace resulting in a local Back Surface Field (BSF). This process sequence yields i-PERC (industry applicable Passivated Emitter and Rear Contact) solar cells.

The dielectric layer on the front (SiN_x:H) was opened by UV-ps laser ablation, the laser speed was kept the same for all the samples, only the laser fluence was changed: 0.69 J/cm² (soft laser) and 1.08 J/cm² (hard laser). Prior to plating, a short HF dip was performed to remove any native oxide in the contact opening areas. Approximately 1 μm of nickel was deposited by Light Induced Plating (LIP) followed by 8–10 μm of electroplated copper. Then the samples were immersed into a silver bath to form a thin silver layer in order to prevent oxidation of the copper. All the plating steps were performed in a commercial in-line plating tool from Meco [11]. Contact sintering was then applied for the full metal plated stack in a nitrogen ambient at 250 °C for few minutes to form a nickel silicide layer, reducing the contact resistance. The cross-section of the final p-PERC cell structure is shown in Fig. 1a.

In this work, thermal ageing, which is considered to be the most detrimental for Cu-based metallizations, is discussed. Ageing experiments are performed in vacuum ambient for temperatures up to 235 °C. Samples are intermediately removed from the oven and measured electrically at various times. They are considered failed if the electrical properties reduce to 95% of the original value. The cells were characterized based on light current-voltage (I-V) measurement and Suns V_{oc} measurements. The I-V data were obtained at 1-sun illumination on a WXS-200S-20 Wacom Electric Co tool. Cells were measured on a temperature controlled Cu block in full contact with the rear surface. Pseudo fill factors (pFF) were extracted from curves of suns versus open circuit voltage (V_{oc}) using Sinton Instruments SunsVoc tester [12].

2.2. Defect visualization and lifetime test structure

In order to characterize defects induced during the contact opening by laser ablation, defect etching is carried out and visualized by a Scanning Electron Microscope (SEM). The analysis has been performed on p-type Si after n⁺ emitter formation, deposition of SiO₂ and SiN_x at the front, followed by laser ablation with various laser fluences: 0.48 J/cm², 0.63 J/cm², 0.72 J/cm², 0.96 J/cm² and 1.43 J/cm². The sample structure for defect inspection is shown in Fig. 1b. Conditions of the emitter doping and dielectric layer deposition were the same as for the

fabrication of the solar cells for thermal ageing test. A standard Wright [13] etch solution was used to delineate the defects. This Wright etch solution was made from concentrated HF: Cr₂O₃: H₂O mixtures at a ratio of 1:0.5:1 and throws in 0.5 unit concentrated HNO₃, 2gr of Cu (NO₃)₂·3H₂O and 1 unit CH₃COOH. This can delineate a wide variety of crystal defects on different surface orientations [13]. Before applying the Wright etch solution, the wafer was cleaned by an SPM solution for 10 min, followed by HF 2% in order to remove any oxide layer, which could be formed during the laser ablation process. Then the Wright etching solution was applied by immersion the wafer to the solution for 20 s. Because the etch rate is different between defective and defect-free area, the defects could be visualized and quantified by using the SEM and Transmission Electron Microscopy (TEM).

For the lifetime test, samples which have a symmetrical structure (Fig. 1b) were made. After POCl₃ diffusion, the wafers were subjected to a dry thermal oxidation step, and the n⁺ emitter was formed on both sides. Afterwards, the samples were capped on both sides with PECVD SiO_x and SiN_x. Subsequently, the contact opening was performed on one side only, using either ps-laser ablation (355 nm) or photo-lithography as reference, both methods with different open area fractions. The total recombination current (J_{tot}) was obtained using quasi-steady-state photoconductance-calibrated photoluminescence (QSSPC-PL, BT Imaging). The J_{o,abl} in the laser ablated region and J_{o,litho} in the lithography patterned area were extracted using the method from [14]. Following this method, at high injection level, J_{o,tot} can be extracted from the slope of 1/τ_{eff} as a function of injection level (Eq. (1)). Then J_{o,open} in the opened area (which is either J_{o,abl} or J_{o,litho}) and J_{o,pass} in the passivated area can be extracted from J_{o,tot} versus the fraction of open area (C_{open}) irrespective of the relative magnitude of bulk recombination and recombination at the passivated surface (Eq. (2))

$$\frac{1}{\tau_{\text{eff}}} = \frac{1}{\tau_{\text{bulk}}} + J_{o,\text{tot}} \frac{N_D + \Delta p}{qn_i^2 W} \quad (1)$$

$$J_{o,\text{tot}} = 2J_{o,\text{pass}} + C_{\text{open}}(J_{o,\text{open}} - J_{o,\text{pass}}) \quad (2)$$

2.3. Deep Level Transient Spectroscopy measurement

For the Deep Level Transient Spectroscopy (DLTS) measurement, completed cells before and after thermal annealing were used. Because the devices have a high leakage current and a capacitance higher than the maximum measurable value of 4 nF, the cells were diced to smaller samples. The dicing was done by using a ns laser from the rear side in order to avoid damage induced by this laser to the p-n junction at the front.

Capacitance DLTS has been performed using a Fourier-Transform-based digital system from PhysTech, with a capacitance bridge operated at a fixed frequency of 1 MHz [15]. A bias pulse from reverse bias to 0 V was typically applied to the substrate (p-base) contact, while the emitter was grounded. The period of the bias pulse selects the emission rate window, which corresponds with the peak maximum in the DLTS spectra for each deep level present in the p-type depletion region, close to the junction. At the same time, a sufficiently long bias pulse was employed to fill all deep levels in the part of the depletion region, selected by the reverse and the pulse voltage. For the used substrate doping density, the information depth amounts to roughly 1 μm to 0.5 μm below the junction. Samples were mounted in a liquid nitrogen flow cryostat, enabling temperature scan DLTS from 75 K to slightly above room temperature (RT) (320 K). At the same time, isothermal frequency-dependent scans at a constant temperature were also performed.

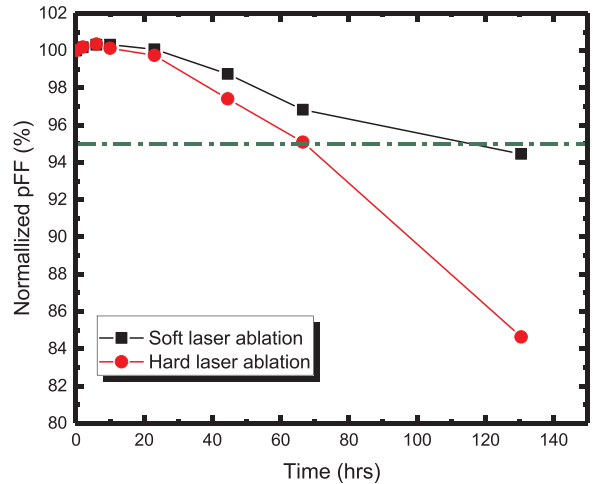


Fig. 3. Monitoring of normalized pFF of various cell types for different ageing times.

3. Results and discussion

3.1. Thermal ageing reliability

Ageing experiments are performed in vacuum ambient for a temperature of 235 °C. The temperature 235 °C was chosen because it is close to the nickel silicide sinter temperature. Samples are intermediately removed from the oven and measured electrically at various times. It is known that if any Ni/Cu would diffuse in during the ageing process, it would first degrade the pFF. The results of pFF versus time are shown in Fig. 3. A clear degradation of the cell performance as a function of the annealing time can be observed. The cells which have the contact opened by hard laser fail faster than the ones using the soft laser. The dark I-V curves of the different types of cells before and after failure are shown in Fig. 4. A striking feature is the hump appearing slightly below 0.3 V (so around the Maximum Power Point) for all types of cells, which correlates with the FF drop after failure by thermal annealing. These humps are the result of the saturation of the Shockley-Read-Hall recombination via the defect levels, which dominate the diode current at low forward bias [16]. A similar observation for Ni plated silicon solar cells after high tempering annealing was reported by Kluska et al. [17].

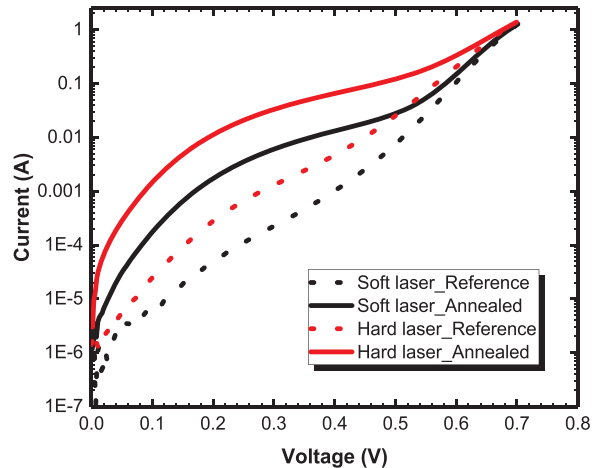


Fig. 4. Dark I-V of difference types of cells before (dotted lines) and after (full lines) ageing.

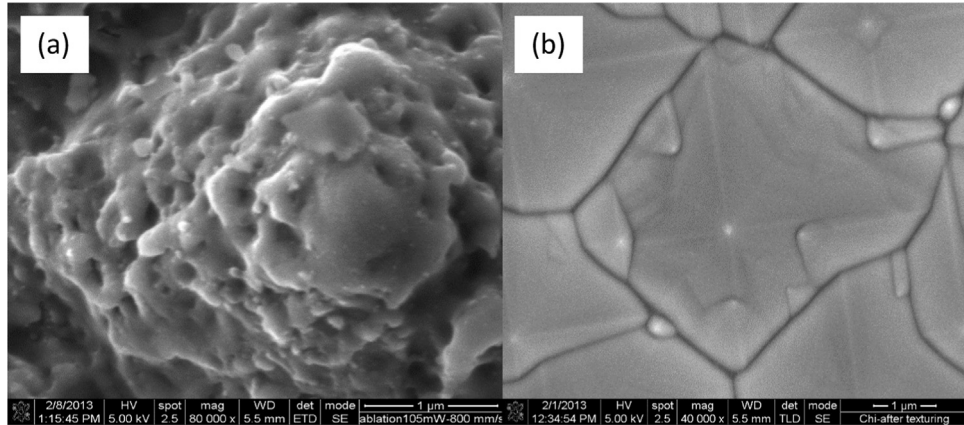


Fig. 5. SEM top view surface morphology: (a) after laser ablation, (b) after photolithography + wet-etching.

3.2. Searching for degradation mechanism

3.2.1. Laser ablation induced defects

It is known that the dielectric layer on top of a silicon substrate is removed in a lift-off caused by stress inside the layer due to increasing vapor pressure of molten silicon after laser irradiation [18]. However, during the selective ablation process, the highly localized heating and rapid cooling of the silicon creates high thermal stresses, which may relax by the introduction of extended defects into the substrate. In order to investigate whether the laser induces defects during the ablation process, samples which have the dielectric either ablated by ps laser or patterned by photolithography were used. SEM images are taken for both cases, before and after Wright etching. The results are collected in Fig. 5 and Fig. 6. Fig. 5a shows a pyramid after the laser ablation.

Silicon melting resulted in a very rough surface while a smooth and sharp surface was observed if the dielectric was opened by a wet-etch method (Fig. 5b). Fig. 6a to d provide a direct comparison of the silicon surface after Wright etching for laser ablated samples at 0.48 J/cm^2 , 0.63 J/cm^2 , 0.96 J/cm^2 and 1.43 J/cm^2 , respectively. It is observed that the preferential etch delineated some crystal defects, which appear as square-shaped pits. In this work, there are almost no defects found between the melted and non-melted areas as Hameiri et al. [19] reported for the laser doping case. This could be due to the fact that laser doping requires a higher laser power in order to simultaneously open the dielectric and drive in the dopants. This would bring a larger thermal expansion mismatch between the irradiated and non-irradiated or heat affected zone, resulting in defects at the contiguous area. The type of defects caused by laser ablation are expected to be dislocations

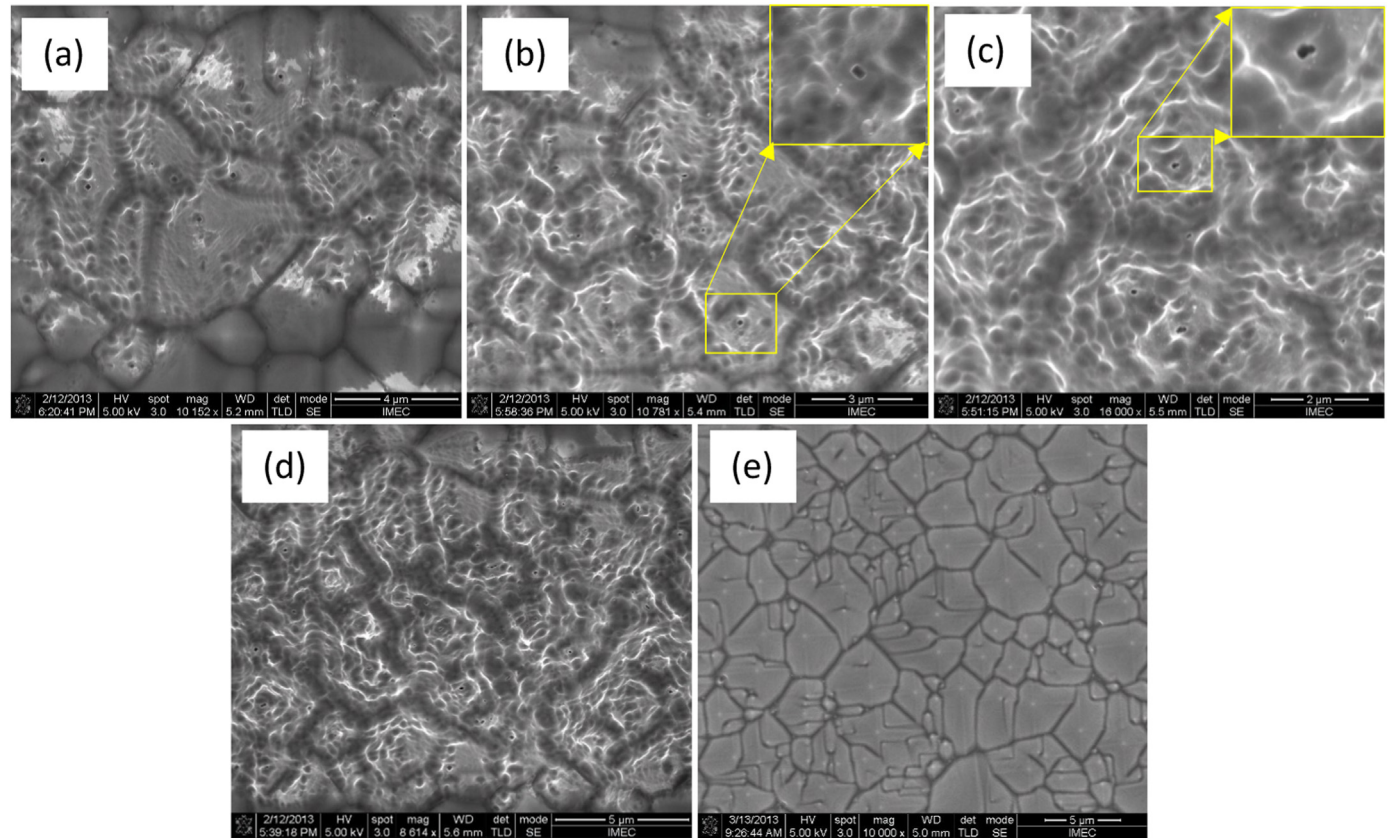


Fig. 6. SEM top view surface morphology: (a), (b), (c), (d) after laser ablation at a fluence of 0.48 J/cm^2 , 0.63 J/cm^2 , 0.96 J/cm^2 , 1.43 J/cm^2 and Wright etching, respectively, (e) after Photo-lithography and Wright etching.

Table 1

Defect density after Wright etching for different contact opening methods and a summary of the J-V measurements.

Method	Laser fluence (J cm ⁻²)	Average defect density (cm ⁻²)	Recombination current (fA cm ⁻²)
Litho			~ 700
Laser ablation	0.48	4 ± 1 × 10 ⁶	
Laser ablation	0.63	7 ± 2 × 10 ⁶	~ 3000
Laser ablation	0.72	7 ± 1 × 10 ⁶	
Laser ablation	0.96	10 ± 2 × 10 ⁶	
Laser ablation	1.43	13 ± 1 × 10 ⁶	

[20]. The dislocations identified here are mostly formed at the pyramid tips what can be simply explained by the fact that the pyramid tip absorbs more energy from the laser beam compared to a flat surface. Using soft laser ablation (Fig. 6a and b) results in quite clear square-shaped pits on the silicon surface, while there are overlapping/distorting pits when a higher laser pulse density is applied (Fig. 6c and d). For the wafer patterned by lithography, the surface looks very smooth and no defects are observed after the Wright etching (Fig. 6e).

In order to quantify the defect density, 3 wafers for each laser fluence were used. After Wright etching, the SEM pictures were taken at three different positions in order to increase the data points and accuracy of the average defect density. As can be seen from Table 1, for all the laser conditions, the defect density is higher than 10⁶ cm⁻² and it increases with increasing laser fluence. The lowest defect density observed is 4 × 10⁶ cm⁻² for the 0.48 J/cm² laser pulse density. However, by using this laser condition, the ablated area is only partially opened which would lead to a high contact resistance issue after metallization. Because of a compromise between the defect density and dielectric opening spot, the laser induced defects are unavoidable. At the insufficient laser fluence required to fully open the dielectric stack, the induced defect density is already at the level of 10⁶ cm⁻². There is no difference in terms of defect density for a laser fluence from 0.63 J/cm² to 0.72 J/cm² while the dielectric is ablated completely. We then divide the laser conditions into 2 groups which are called soft and hard laser. The soft laser corresponds with a fluence lower than 0.72 J/cm², and the hard laser fluence is higher than 0.96 J/cm².

In order to identify more clearly the crystal defects that are visible in the SEM images, a TEM analysis is performed on Wright-etched samples. The TEM images of a pit at the top of a pyramid after 0.96 J/cm² laser ablation are shown in Fig. 7. Our textured surfaces are produced by TMAH chemical etching and feature random pyramids with different size and height. The pits induced due to the laser ablation process appear not on every pyramid tip but scattered along the ablation area. The pit appears quite deep for this laser fluence as can be seen in the magnified view of Fig. 7b. The crystal defect is most likely a

dislocation observed around 1.3 μm below the surface of the pit. As there are no defects found for the case of using photolithography followed by wet etching, the dislocations are proven to be caused by the laser ablation process. An impact of the dielectric deposition or TEM preparation is excluded. Hermann et al. [21] reported dislocations found on both the sidewalls and the tips of the pyramid when applying a ps laser ablation on textured silicon, while there were no defects observed for the planar surface. This was explained by the different crystal orientation. Please note that, in our case the apexes of TMAH textured (100) silicon wafers usually are (100) oriented, while the pyramid sidewalls are (111) oriented. Moreover, the distinct crystal damage in the apex might be caused by thermo-mechanical stresses propagating symmetrically from the pyramid sidewalls and meeting at the pyramid tip. The quite deep dislocations into the silicon together with the shallow emitter (500 nm deep) would lead to damage inside the Space Charge Regions (SCRs) of the p-n junctions.

Our previous work measured the recombination current at the opened area by QSSPC and has compared mask opening by photolithography followed by a wet etching (defect-free) and soft laser ablation [22]. The results are summarized in Table 1. It has been found that the recombination current at the laser ablated area is 3000 fA/cm², which is almost 4 times higher than the recombination current at the area opened by photolithography and wet etch. This data proves that the dislocations generated from laser ablation can act as recombination centers and drastically reduce the effective lifetime.

3.2.2. Ni/Cu migration

It is well known that defects arising from impurities, grain boundaries, etc. result in the creation of traps which capture free electrons and holes. Even at low concentrations these trapping centers can alter the semiconductor device performance. Detecting and mitigating these traps in Photovoltaic devices, especially in high efficiency solar cells are important. In our work, DLTS was carried to study the electrically active defects in the base depletion region of the p-n junction. Fig. 8 shows some of the temperature (T-) scan DLTS-spectra for the soft and hard laser ablation before and after ageing, obtained while warming up the samples from 75 K to room temperature and applying the same bias pulse.

As can be seen in Fig. 8, some positive peaks are found for both samples, which typically correspond to majority carrier, i.e., hole traps in the p-type silicon depletion region. The shallow peak H1 at 80 K is revealed for all samples both soft and hard laser and before and after annealing. It strongly suggests that this trap level is probably induced during the cell processing. At the same time, the peak amplitude, which is proportional to the trap concentration, is about 10 times higher for the hard laser (Fig. 8b) compared with the soft laser treatment (Fig. 8a). This indicates the role played by the laser ablation in the introduction

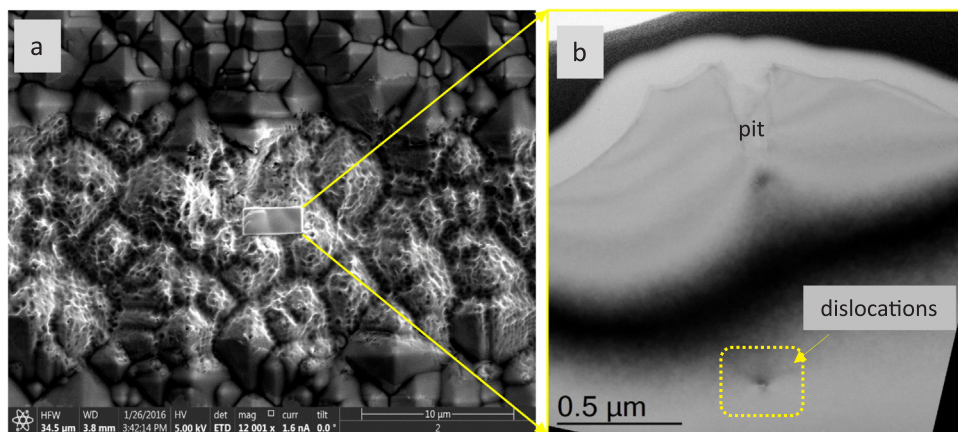


Fig. 7. TEM images of a Wright-etch pit at the pyramid top after 0.96 J/cm² laser ablation. A magnified view of the selected area in (a) is presented in b.

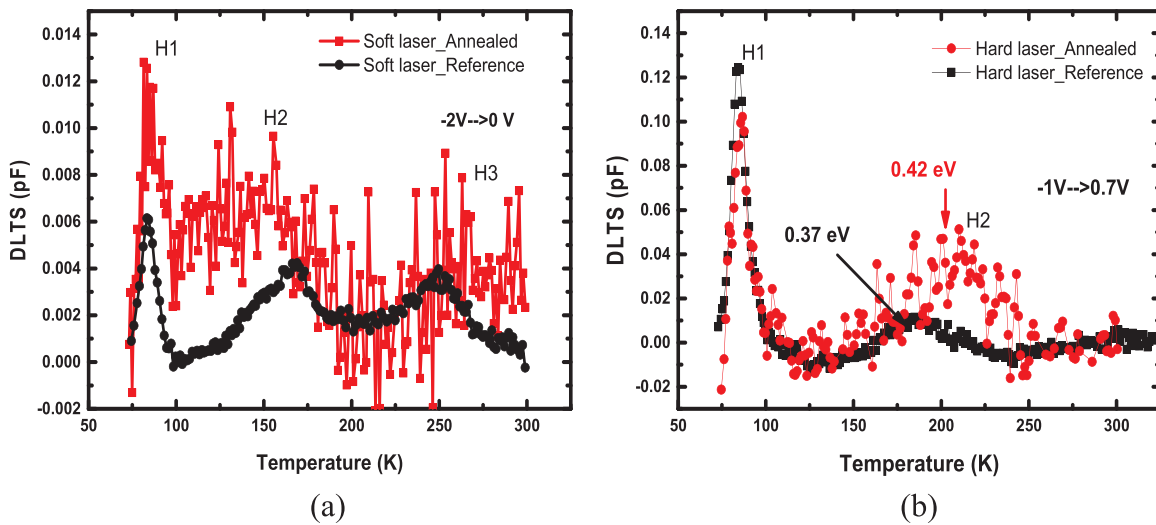


Fig. 8. DLTS spectra before and after annealing for soft-laser (a) and hard-laser (b) annealed solar cells.

of nickel in the silicon p-type base region. Thermal ageing, on the other hand, appears to have a marginal impact on the H1 DLTS amplitude.

The activation energy of this trap can be extracted from the emission rate for holes in p-type silicon e_h :

$$e_h = \frac{1}{\tau} = \sigma_p \beta T^2 \exp \left\{ - \frac{(E_T - E_v)}{kT} \right\} \quad (3)$$

where τ : emission time constant (s)

σ_p : Capture cross section of holes (cm^2)

β : Pre factor ($s^{-1}cm^{-2}K^{-2}$)

$(E_T - E_v)$: Activation en

Thermal Conductivity

$$\ln(\tau T^2) = -\ln(\beta \sigma_p) + \frac{E_T - E_v}{kT} \quad (4)$$

An Arrhenius plot of the peak maximum position obtained for the different spectra of all the laser-ablated samples for the hole trap observed around 80 K is shown in Fig. 9a. There is quite a good agreement of the H(80 K) data for the different samples, suggesting this peak corresponds to the same trap level.

From the slope of the least-squares fit line, an average activation energy of 0.178 eV is derived, which means that the deep level

belonging to H(80 K) locates around 0.178 eV from the valence band maximum in the p-type silicon base. Based on the small hole capture cross section derived from an Arrhenius plot, it is concluded that the trap acts as a donor level and could belong to either substitutional Cu (Cu_s) at 100 K [23] or substitutional Ni (Ni_s) at 80 K [24], which are donor levels in p-type silicon. In order to identify the origin of this hole trap more accurately, a comparison of the Arrhenius plot of the peak H (80 K) from our samples (exp.data) and the literature data for substitutional Ni and Cu is performed and shown in Fig. 9b. It suggests that level H(80 K) corresponds to the substitutional nickel donor level, since there is a good overlap of both Arrhenius plots. This peak appears in all the samples, before and after thermal ageing, which means the nickel diffuses in already after the plating and sinter step. The Ni contamination from the bulk silicon wafers in this case can be excluded.

The concentration of active Ni_s may be derived from the height of the DLTS peak, provided a sufficiently long bias pulse is employed [25]. Note that there is a difference in the vertical scale in Fig. 8a and b. It is clearly seen that the height of the peak H(80 K) for the hard laser ablated sample is 10 times higher than for the soft laser ablation. This means that the concentration of Ni diffusing in the Si bulk is higher when using hard laser ablation compared to the soft laser ablated sample. The concentration of Ni is estimated at the level of 10^{11} – 10^{12} atom/cm⁻³, which is rather low. However, especially in high-efficiency solar cells this level of Ni_s is considered as an efficient recombination

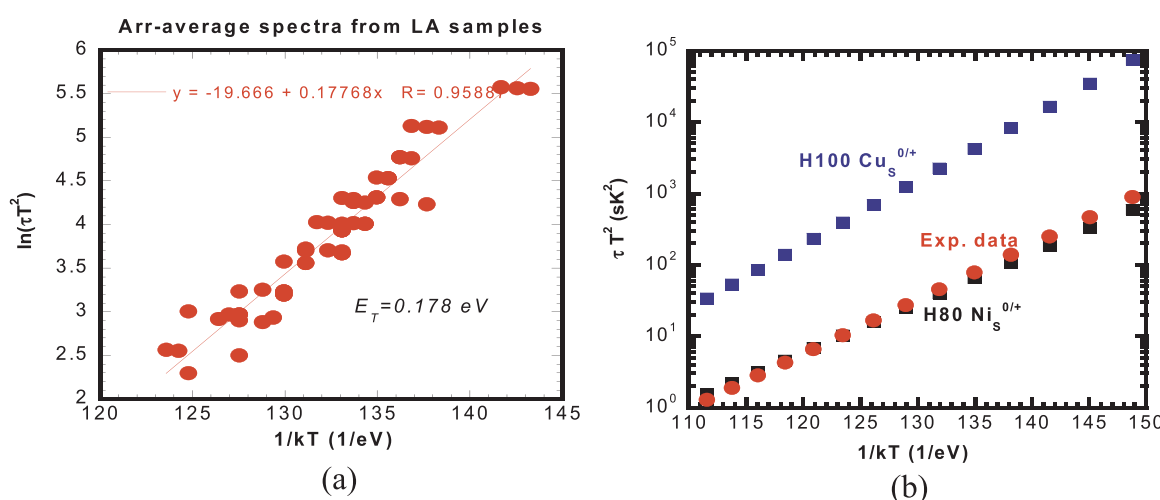


Fig. 9. Arrhenius plot of the peak H(80 K) (a) and comparison with the Arrhenius plot for Cu_s and Ni_s (b).

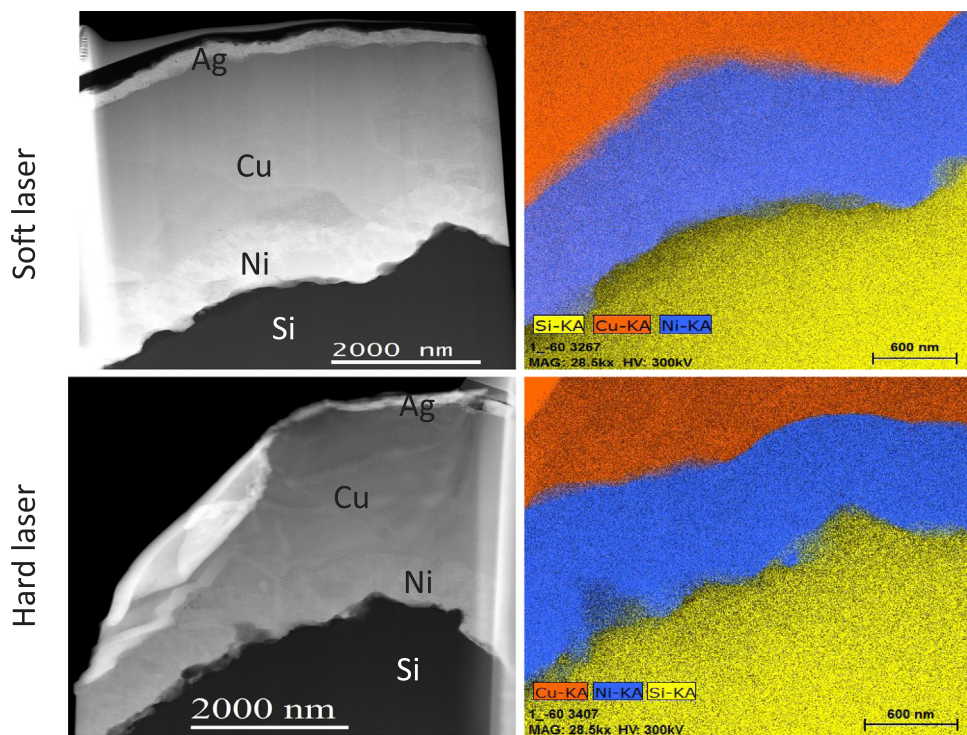


Fig. 10. TEM images of laser ablated samples before ageing at 235 °C.

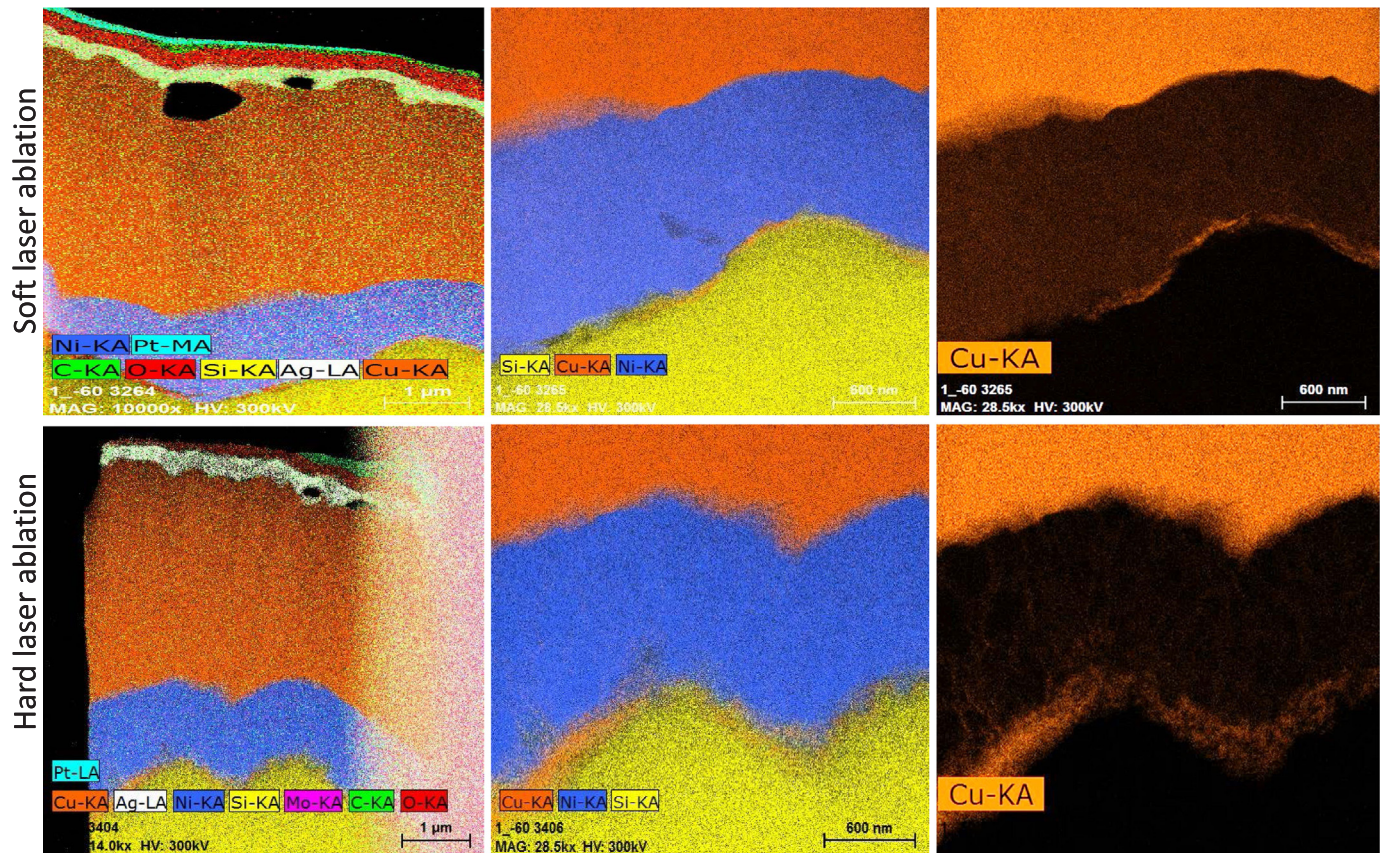


Fig. 11. TEM images of the Cu/Ni/Si stack after ageing at 235 °C.

center when it decorates extended defects like dislocations [26]. Evidence for that mechanism is given in Fig. 8b, showing the presence of a dislocation-related level around 180 K, which is absent for the soft laser diode. In addition, thermal ageing yields a further increase of the trap

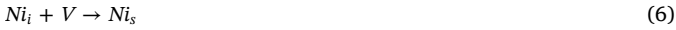
concentration and a shift of the 180 K level toward mid-gap, corresponding with an increase of the activation energy from 0.37 eV to 0.42 eV. This is typical what is observed for an extended defect, suffering from a higher metal decoration [26]. At the same time, it has

been shown that the recombination activity of a heavier decorated dislocation increases, which could well explain the higher recombination current in Fig. 4 after ageing. In the work of Kluska et al. [17], a hump appeared in the dark I-V causing a degradation of the pFF of plated Ni/Ag solar cells. It was assumed to be caused by the local formation of Ni silicide spikes into the space charge region during the tempering. In our case, there is no evidence of Ni silicide spikes in Figs. 10 and 11, which suggests a well-controlled sintering conditions. The non-ohmic shunts lowering the pFF after annealing could be explained by the presence of dislocations induced by laser ablation together with decoration by nickel (metal) diffusion.

Early studies already demonstrate the fast diffusion of nickel in silicon, typical for interstitial atoms [27–30]. Moreover, it has been shown that during a Ni-silicidation process nickel diffuses in the silicon substrate already at the initial stages of the process [31,32]. The diffusion coefficient of Ni_i is given by [30] for the temperature range between 250 °C and 350 °C.

$$D = 10^{-13} \exp\left(-\frac{0.27}{kT}\right) \quad (5)$$

Substitutional nickel is the minority but electrically active configuration in silicon and forms through an exchange or dissociative mechanism of the kind [27,28]:



With Ni_i a fast diffusing interstitial species. The effective diffusion will be governed by the reaction of vacancies V with appropriate sinks/sources. In dislocated silicon, both the surface and the dislocations can act as a source of vacancies. This means that the site exchange mechanism depends on the dislocation density. This could explain why there is more Ni_s found for the hard laser ablated samples than for soft laser ablated cells. Note that the DLTS method detects only the electrically active species, in this work Ni_s . There are probably more inactive interstitial Ni atoms diffused in, which could form nickel precipitates and further degrade the solar cell performance by decorating the extended defects in the p-type base during ageing.

There is no substitutional copper detected in the silicon substrate, within the DLTS detection limit of 10^{11} cm^{-3} , as can be seen in the Fig. 9b as well, since there is no Cu_s peak at 100 K. In fact, crystalline silicon solar cells can tolerate rather large amounts of copper contamination, up to 10^{17} cm^{-3} during CZ crystal pulling [33], before a noticeable degradation of the performance occurs. At the same time, it is one of the few metal impurities which is more recombination active when precipitated, compared with dissolved as substitutional or interstitial impurity. It is believed that copper precipitation in p-type silicon gives rise to the so-called copper Light-Induced-Degradation [34]. The work from R. Labie on thermal ageing for Physical Vapor Deposition (PVD) of Ti/Cu considered copper diffusion as a critical issue for solar cell degradation. However, no proof of the presence of copper in the silicon bulk was reported [35]. It should be noted here that Cu_s is usually only a fraction (< 1%) of the total solid solubility of copper in silicon; the main fraction being in interstitial lattice sites [6]. The latter cannot be detected by DLTS, so that we have to be careful in drawing conclusions about the potential impact of copper on the reliability of the solar cells studied. Perhaps Cu-LID experiments can further enlighten this issue.

The other two semi-shallow hole traps at 170 K and 250 K in Fig. 8a could correspond to interstitial carbon-interstitial oxygen (C_iO_i) complexes from the silicon substrate. Interestingly, there is a quite broad peak, which typically corresponds to extended defects, like dislocations in silicon, observed around 180 K for the hard-laser-ablated samples (Fig. 8b). There is no such broad peak found in the soft laser ablated diode. This could originate from the fact that the dislocations generated by soft laser power are shorter and mostly stay within the n^+ emitter, while the DLTS technique detects the defects extending in the Si p-type bulk side, i.e., in the depletion region. Our previous work [22] reported

the depth of defects induced by soft laser ablation being less than 0.5 μm (emitter depth), while the defects generated by hard laser ablation can penetrate into the silicon bulk. Fig. 8b also shows a comparison of the H180K peak before and after annealing. This peak shifts to a higher temperature (200 K) and has a higher amplitude after thermal ageing. The energy of this peak is calculated to be around 0.42 eV at 200 K after annealing, which is closer to the silicon mid-gap, meaning this deep level becomes more harmful for the solar cells. As discussed before, the shifting of this deep level could be due to more decoration by metal impurities, i.e., nickel, at the dislocations [26].

A TEM analysis was performed of the Ag/Cu/Ni/Si stack for the laser ablated samples before and after ageing. Some of the TEM images for the reference samples are shown in Fig. 10. The metal stack is clearly seen for both types of samples in the STEM image on the left hand side, with the thin Ag as capping layer, on top of around 5 μm of Cu and a 1 μm Ni layer. The more flattened pyramid and rough surface is also obviously seen for the hard laser ablated sample, compared to the soft laser ablated one.

Fig. 11 shows TEM images of the Cu/Ni/Si interface for the soft and hard laser ablated samples after ageing at 235 °C. Copper migrates through the Ag layer, forming a CuO_x layer on top of the metal stack after the ageing for both samples. The CuO_x layer formed could due to the fact that the samples were taken out for electrical measurement from time to time until they were failed. It was also visually seen by eyes that the color of the fingers and busbar changed due to this migration. This yields some voids at the interface of the Ag/Cu layers as can be observed in Fig. 11. These voids are called Kirkendall voids, which form when two adjacent metals with different diffusion coefficients are annealed. Similar behavior for an Ag/Cu/Ni stack has been reported by Lee et al. [36]. After annealing, Cu diffused into the vacancies of the Ag layer, the vacancies move to the Cu layer. If there is no sinks in the Cu layer to absorbed these vacancies, they will be supersaturated, which causes the voids to nucleate at the interface of Cu/Ag [37]. Cu is also found at the Ni/Si interface after ageing at 235 °C for the laser-ablated samples. It seems that copper has diffused through the nickel layer, since copper is also seen in the nickel layer as shown in Fig. 11. It is well known that copper has a tendency to stay at the silicon surface. The segregation of copper in a p^+ silicon substrate is known as p/p^+ gettering and explained by the difference in the Fermi level position in the p-layer and p^+ substrate combined with a higher probability of CuB pair formation in the p^+ substrate than in the p-layer [6]. In our case, copper, mostly present as interstitial Cu_i is segregated at the n^+ silicon surface, which could be because of the repulsion by P^+ ions in the n^+ layer. Moreover, the Fermi level position in n^+ silicon close to the conduction band renders Cu_i neutral and favors precipitation [6]. It is difficult to quantify the amount of copper migration due to the rough surface, however, it seems there is more copper segregated at the Ni/Si interface for the hard laser-ablated sample after annealing than for the soft-laser ablated one. This might be related to more Ni diffused in the silicon base for the hard laser samples, leaving more vacancies for Cu_i to go through this layer and agglomerate at the Ni/Si interface. The electromigration of copper has been well investigated as one of the failure mechanisms in the Cu line for advanced microelectronics interconnections [38] resulting in voids and, therefore, a higher resistance. In solar cells, further investigation of the impact of copper migration needs to be carried out. The same work for lower thermal annealing temperature is on-going to see if this behavior happens in the real-life operation of silicon solar cells. There is no copper found in the silicon layer (emitter and substrate) from both DLTS signals and TEM results for both reference and aged samples.

A short summary of the findings of this investigation is shown in Table 2. Both types of cells show the degradation of the pFF as a dominant factor. The hard laser-ablated cells have a lower cell performance due to a higher dislocations density induced by the laser ablation and penetrating in the p-type base region. This is accompanied by a higher concentration of active Ni atoms diffused in after the sintering

Table 2

Summary of the main observations for the soft and hard laser-ablated solar cells.

		Soft laser	Hard laser	Comments
DLTS	pFF (%)	78.1	74.1	An average pFF Pre-annealing
	n (%)	19.6	18.2	An average n Pre-annealing
	Laser induced defects	yes	yes	Dislocations, Higher density and deeper in the HLA
	H80K	yes	yes	Ni diffused in. Higher Ni _s found for the HLA
	H170K	yes	no	C _x O _i
	H220K	no	yes	Dislocations, shifts after ageing
TEM	H250K	yes	no	C _x O _i
	Cu migration	yes	yes	Seems more Copper diffused in for the HLA samples

step. Ageing results in an increase in the recombination activity of the dislocations by a further decoration by in-diffusing metal atoms. This gives rise to a shift of the activation energy toward mid-gap and a higher forward recombination current in the solar cells. This also causes a faster cell degradation after thermal ageing of the hard ablated cells compared to the soft laser-ablated counterparts. The Cu migration and segregation at the silicon surface happens in both types of samples, with more Cu seen at the interface for the hard laser ablated case, which could contribute to the degradation of the devices as well.

4. Conclusion

We have investigated the reliability of plated Ni/Cu/Ag metallization stacks for c-Si solar cells. The laser ablation used to open the dielectric layer before plating is shown to introduce dislocations. The dislocation density depends on the laser fluence, higher laser fluence results in a higher dislocation density, penetrating deeper in the silicon substrate into the p-type base. These dislocations are visualized by defect etching followed by a combined SEM and TEM analysis. It is found that the dislocations do indeed increase the forward recombination current of the silicon n⁺ p solar cells. A higher laser fluence degrades the solar cell performance more. The dislocations induced by laser ablation give rise to a broad hole trap in DLTS for the hard laser-ablated diode. We also have found that there is nickel diffused in during the cell processing, most likely after the plating and sintering step. The concentration of active substitutional nickel (Ni_s) is found at the level of 10¹¹–10¹² atom/cm³. Copper migration and segregation at the silicon surface has been observed for samples after ageing at 235 °C. Copper diffuses through the Ag layer, forming a CuO_x layer on top of the Ag layer and giving rise to large voids at the Cu/Ag interface. Copper is also detected by TEM at the Ni/Si interface suggesting copper migrates through the Ni layer and segregates at the silicon surface. There is no copper seen (within the level of 10¹¹ atom/cm³ for DLTS) inside the n⁺ emitter and silicon base by TEM and DLTS even after thermal ageing at 235 °C. The impact of copper migration on the cell performance needs to be further investigated. Similar work for lower temperature ageing is on-going to define if the Cu migration would occur at the real-life operation as well.

Acknowledgements

The authors would like to thank R. Russell for plating the p-PERC solar cells in this study, as well as L. Tous and M. Recaman for assistance with processing and discussion. The support of the characterization group is also deeply acknowledged.

References

- [1] C. Muschelknautz, A. Henning, et al, Standard Printing Techniques – Pushing the Envelope to 75 mg Paste per Cell, in: Proceedings of the 4th metallization workshop.
- [2] T. Falcon, Ultra-fine Line Printing for Silicon Solar Cells: Mesh Screens or Metal Stencils? in: Proceedings of the 3rd Metallization workshop, 2011.
- [3] A.A. Istratov, C. Flink, E.R. Weber, Impact of the unique physical properties of copper in silicon on characterization of copper diffusion barriers, Phys. Status Solidi B 222 (2000) 261–277.
- [4] J.S.H. Chao, H. Kang, S.S. Wong, Y. Shacham-Diamand, Electroless Cu for VLSI, MRS Bull. 18 (1993) 31–38.
- [5] L. Tous, J.-F. Lerat, T. Emeraud, et al., Nickel silicide formation using excimer laser annealing, Energy Procedia 27 (2012) 503–509.
- [6] A.A. Istratov, E.R. Weber, Physics of copper in silicon, J. Electrochem. Soc. 149 (2002) G21–G30.
- [7] J. Bartsch, A. Mondon, K. Bayer, C. Schetter, M. Hörteis, S.W. Glunz, Quick determination of copper-metallization long-term impact on silicon solar cells, J. Electrochem. Soc. 157 (2010) 942–946.
- [8] S. Flynn, A. Lennon, Copper penetration in laser-doped selective-emitter silicon solar cells with plated nickel barrier layers, Sol. Energy Mater. Sol. Cells 130 (2014) 309–316.
- [9] A. Kraft, C. Wolf, J. Bartsch, M. Glatthaar, Characterization of copper diffusion in silicon solar cells, Energy Proc. 67 (2015) 93–100.
- [10] A. Kraft, C. Wolf, J. Bartsch, M. Glatthaar, S. Glunz, Long term stability of copper front side contacts for crystalline silicon solar cells, Sol. Energy Mater. Sol. Cells 136 (2015) 25–31.
- [11] Meco Plating system. <<https://www.besi.com/products-technology/product-details/product/meco-cpl/show/>> (Accessed 6 November 2017).
- [12] R. A. Sinton, A. Cuevas, A quasi-steady-state open-circuit voltage method for solar cell characterization, in: Proceedings of the 16th European PVSEC (2000) pp. 1152–1155.
- [13] M.W. Jenkins, A new preferential etch for defects in silicon crystals, J. Electrochem. Soc. 124 (1997) 757–759.
- [14] J. Deckers, X. Loozen, N. Posthuma, B. O'Sullivan, M. Debucquoy, S. Singh, M. Aleman, M. Recaman, I. Gordon, P. Verlinden, R. Mertens, J. Poortmans, Injection dependent emitter J₀ measurement under metallized areas using Photoconductance Decay, in: Proceedings of the 28th European PVSEC (2013) pp. 806–810.
- [15] S. Weiss, R. Kassing, Deep level transient Fourier spectroscopy (DLTSF) – A technique for the analysis of deep level properties, Solid-State Electron 31 (1988) 1733–1742.
- [16] S.J. Robinson, A.G. Aberle, M.A. Green, Recombination saturation effects in silicon solar cells, IEEE Trans. Electron Devices 41 (1994) 1556–1569.
- [17] S. Kluska, C. Fleishmann, A. Buchler, et al., Micro characterization of laser structured solar cells with plated Ni-Ag contacts, Sol. Energy Mater. Sol. Cells 120 (2014) 3323–3331.
- [18] G. Heinrich, M. Bahr, K. Stolberg, T. Wutherich, M. Leonhardt, A. Lawerenz, Investigation of ablation mechanisms for selective laser ablation of silicon nitride layers, Energy Procedia 8 (2011) 592–597.
- [19] Z. Hameiri, T. Puzer, L. Mai, A.B. Sproul, S.R. Wenham, Laser induced defects in laser doped solar cells, Prog. Photo. Res. Appl. 19 (2011) 391–405.
- [20] Atlas for characterization of defect in silicon. Siltronic, Postfach, Germany, 2004.
- [21] S. Hermann, T. Dezhdar, N.P. Harder, R. Brendel, M. Seibt, S. Stroj, Impact of surface topography and laser pulse duration for laser ablation of solar cell front side passivating SiN_x layers, J. Appl. Phys. 108 (1–8) (2010) 114514.
- [22] C. Dang, R. Labie, L. Tous, R. Russell, M. Recaman, J. Deckers, A. Uruena, F. Duerinckx, J. Poortmans, Investigation of laser ablation induced defects in crystalline silicon solar cells, Energy Procedia 55 (2014) 649–655.
- [23] S. Knack, J. Weber, H. Lemke, H. Riemann, Copper-hydrogen complexes in silicon, Phys. Rev. B 65 (2002) 1–8 (165203).
- [24] L. Scheffler, V.I. Kolkovsky, J. Weber, Electrical levels in nickel doped silicon, J. Appl. Phys. 116 (2014) 1–8 (173704).
- [25] E. Simoen, J. Lauwaert, H. Vrielinck, Analytical Techniques for Electrically Active Defect Detection, Semiconductors and Semimetals, Eds L. Romano, V. Privitera, C. Jagadish, 91 (2015) pp. 205–250.
- [26] V. Kveder, M. Kittner, W. Schroter, Recombination activity of contaminated dislocations in silicon: a model describing electron-beam-induced current contrast behavior, Phys. Rev. B 63 (2001) 1152081–11520811.
- [27] M. Yoshida, K. Saito, Dissociative diffusion of nickel in silicon and self-diffusion of silicon, Jpn. J. Appl. Phys. 6 (1967) 573–581.
- [28] H.P. Bonzel, Diffusion of nickel in silicon, Phys. Status Solidi 20 (1967) 493–504.
- [29] G.L.P. Berning, K.H. Yoon, G. Lewis, S. Sinharoy, L.L. Levenson, The observation of pseudodiffusion of nickel in single-crystal silicon by in-depth Auger electron spectroscopy, Thin Solid Films 45 (1977) 141–145.
- [30] M.K. Bakhtyarkhanov, S. Zaïnabidinov, A. Khamidov, Some characteristics of diffusion and electrotransport of nickel in silicon, Sov. Phys. Semicond. 14 (1980) 243.
- [31] M. Tsuchiaki, K. Ohuchi, C. Hongo C, Junction leakage generation by NiSi thermal instability characterized using damage-free n⁺ /p silicon diodes, Jpn. J. Appl. Phys. 43 (2004) 5166–5173.
- [32] M. Tsuchiaki, A. Nishiyama, Substrate orientation dependence of NiSi junction leakage induced by anisotropic Ni migration in crystal Si, Jpn. J. Appl. Phys. 46 (2007) 1830–1840.
- [33] J.R. Davis Jr, A. Rohatgi, R.H. Hopkins, P.D. Blais, P. Rai-Choudhury, J.R. McCormick, H.C. Mollenkopf, Impurities in silicon solar cells, IEEE Trans. Electron Devices ED 27 (1980) 677–687.

- [34] H. Vahlman, A. Haarahiltunen, W. Kwapisil, J. Schön, A. Inglese, H. Savin, Modeling of light-induced degradation due to Cu precipitation in p-type silicon. II. Comparison of simulations and experiments, *J. Appl. Phys.* 121 (2017) 1–11 (195704).
- [35] R. Labie, J. L. Hernandez, J. Govaerts et al., Cu plated i-perc cells: ageing and humidity reliability tests, in: Proceedings of the 26 European PVSEC (2011) pp. 1195–1198.
- [36] S. Lee, D. Lee, A. Rehman, et al., Study of annealing temperature for Ni/Cu/Ag plated front contact single crystalline solar cells, *IEEE J. Photovolt.* 6 (2016) 1090–1093.
- [37] T.C. Liu, C.M. Liu, Y.S. Huang, et al., Eliminate Kirkendall voids in solder reactions on nanotwinned copper, *Scr. Mater.* 68 (2013) 241–244.
- [38] S. Bayne, K. Croes, I.D. Wolf, Z. Tokei, 1/f noise measurement for faster evaluation of electromigration in advanced microelectronic interconnections, *J. Appl. Phys.* 119 (2016) 1–9 (184302).